

Origin of dissolved gas (CO₂, O₂, N₂, alkanes) in pore waters of a clay formation in the critical zone (Tégulines Clay, France)

Catherine Lerouge^{a,*}, Mathieu Debure^a, Benoit Henry^a, Ana-Maria Fernandez^b,
Michaela Blessing^a, Eric Proust^a, Benoit Madé^c, Jean-Charles Robinet^c

^a BRGM, 3 Avenue Claude Guillemin, 45060, Orléans Cédex 2, France

^b CIEMAT, Departamento de Medio Ambiente, 28040, Madrid, Spain

^c ANDRA, 1-7 Rue Jean-Monnet, 92298, Châtenay-Malabry Cedex, France

ARTICLE INFO

Editorial handling by Thomas Gimmi

Keywords:

Chemical weathering

Critical zone

Pore waters

Dissolved gas

Carbon stable isotopes

Tégulines clay

Reactive transport modeling

ABSTRACT

Understanding weathering processes in clay formations is an issue of primary importance for the preservation of our natural environment. Reactive-transport modeling used to simulate weathering of clay formations has indicated that reactive gases (CO₂ and O₂) are major parameters in controlling weathering processes.

The Lower Cretaceous Tégulines marine-clay formation outcropping in the area of Brienne-le-Chateau (north-eastern France) has been investigated in the context of a sub-surface waste repository. We developed gas monitoring (CO₂, O₂, N₂, alkanes) of core samples from two boreholes that entirely crosscut the Tégulines Clay formation, to define the consequences of weathering and oxidation processes on gases dissolved in pore waters. We discuss amounts of gas and the carbon isotopic composition of CO₂ in terms of pore water chemistry including dissolved-inorganic carbon (DIC) and alkalinity, mineral reactivity, organic-matter degradation and oxygen diffusion. Degassing of samples conditioned under He atmosphere provided evidence of very high CO₂ production in the soil (0–30 cm), and high CO₂ degassing associated with a high oxygen level in the first 2–10 m of the clay. The CO₂ degassing increase observed in weathered clay relative to preserved clay resulted from calcite dissolution due to pyrite oxidation and organic matter degradation. The δ¹³C of CO₂ indicates that organic matter degradation was a major source of CO₂ at shallow depths and down to 10–12 m, which is the maximum depth at which we observed fossil roots. Then the CO₂ degassing decreased down to a constant value in preserved clay, where the carbonate system and the mineral assemblage control dissolved carbonates in pore waters. The profile of the δ¹³C_{CO2} also provides evidence of progressive CO₂ diffusion of organic origin from the underlying Greensands aquifer in the lower part of Tégulines Clay up to ~40 m in the AUB230 borehole.

As a first step toward understanding interactions between Tégulines Clay and near surface waters or water at the Greensands interface, we developed a reactive-transport model to simulate in one dimension weathering processes under ambient temperature, constrained by geochemical reactions in soil (organic matter degradation) and in the clay (pyrite oxidation and calcite dissolution), exchange, DIC and pore water chemistry. The simulation was carried out for 10 kyrs, assuming that weathering and soil formation began after the last glacial maximum. The DIC profile cannot be simulated without considering evaporation processes in agreement with the isotopic data. This type of approach combining a complete field dataset (reactive-gas concentrations, δ¹³C of CO₂, major-ion concentrations, δ¹⁸O and δD of pore waters) and reactive-transport modeling is necessary for better understanding of chemical weathering processes in the critical zone.

1. Introduction

The critical zone (CZ) extends from vegetation to groundwater and is a system that combines chemical, biological, physical, and geological processes supporting life all together (Brantley et al., 2007, 2013;

Sullivan et al., 2016; White et al., 2015). Among the various lithologies, marine-clay formations represent ~25% of the continental surface. They are of peculiar interest due to their low permeability, complex fluid and gas transfers (slow vertical diffusion/lateral transfer), buffer capacity associated with carbonate minerals, and early diagenetic mineral

* Corresponding author.

E-mail address: c.lerouge@brgm.fr (C. Lerouge).

<https://doi.org/10.1016/j.apgeochem.2020.104573>

Received 26 August 2019; Received in revised form 13 March 2020; Accepted 14 March 2020

Available online 19 March 2020

0883-2927/© 2020 Elsevier Ltd. All rights reserved.

assemblages. These are largely controlled by microbial activity and are consequently redox sensitive (Duffy et al., 2014; Lerouge et al., 2011, 2014). Interactions between marine-reduced clay formation, atmosphere and hydrosphere induce mineral, chemical, pore water, petrophysical and mechanical changes in the clay formation (Brantley et al., 2013; Lerouge et al., 2018; Soulet et al., 2018a; Sullivan et al., 2016; Yesavage et al., 2012 and references therein). Most of these interactions and changes are driven by biological activity, including macro- and micro-organisms, and vegetation. Clay-rock reactivity includes pyrite oxidation and sulfur state/pH changes, carbonate dissolution/alkalinity/DIC changes, organic matter degradation/DOC changes (Debure et al., 2020; Dideriksen et al., 2007; Drake et al., 2009; Duffy et al., 2014; Lerouge et al., 2018; Mazurek et al., 1996; Soulet et al., 2018a), and changes in other redox proxies (Tostevin et al., 2016; Yu et al., 2017). The progression of the weathering and oxidizing fronts is controlled by 1) the meteoric water influx rate, 2) oxidation reaction kinetics (pyrite oxidation, organic matter degradation), and 3) oxygen flux (Bolton et al., 2006; Brantley et al., 2013; Li et al., 2017). While numerous data are available on mineral reactions and pore water chemistry in the critical zone, little are available on gas transfer through the vadose zone and are essentially obtained by reactive-transport modeling (Hasenmueller et al., 2017; Heidari et al., 2017).

Among scientific research on radioactive-waste disposal in deep geological clay formations, a core degassing methodology has been developed to monitor degassing in reduced-marine claystone conditioned in gas containers under helium just after sampling (Girard et al., 2005). The numerous degassing experiments carried out on cores of reduced-marine claystone (Callovian-Oxfordian Clay, Opalinus Clay, Toarcian shales of Tournemire) provided evidence of CO₂ and alkane steady state being attained after few months, and a relatively homogeneous range of CO₂ partial pressures (P_{CO2}) between 6 and 12 mbar (Gaucher et al., 2010; Lerouge et al., 2015; Wersin et al., 2016). The δ¹³C of the degassed CO₂ and of calcite separated from the claystone confirmed the thermodynamic equilibrium between carbonate solution species and calcite (Gaucher et al., 2010; Girard et al., 2005; Lerouge et al., 2015).

In this paper, we applied and developed the core degassing methodology to the Tégulines Clay of the Lower Cretaceous age that outcrops in the north-eastern part of the Paris Basin in France. For a decade, Tégulines Clay was investigated in the context of surface repository for low-level radioactive waste (Debure et al., 2020; Debure et al., 2018; Duffy et al., 2014; Lerouge et al., 2018). Chemical, mineral and petrophysical characterization of core samples from two drilling campaigns in 2013 and 2015 provided evidence of weathering and oxidation processes down to ~20 m depth (Lerouge et al., 2018). Due to the significant mineral and pore-water changes including the perturbation of the carbonate system, it is of major interest to investigate the consequences of weathering and oxidation processes on core degassing in Tégulines Clay. We monitored CO₂, O₂, N₂ and alkanes degassed by core samples from three boreholes crosscutting the clay down to the Greensands aquifer, providing dissolved gas data through the critical zone. Amounts of gas, carbon isotopic composition of CO₂ and reactive transport modeling are discussed in terms of pore water chemistry, CO₂ origins, gas transfer, and key parameters for the understanding of weathering processes in the critical zone.

2. Geological setting and sampling

2.1. Geological setting

The Gault clay formation in the Aube department in the eastern part of the Paris Basin consists of siliciclastic shales deposited in an open marine environment from Middle to Upper Albian (Lower Cretaceous) on the Greensands formation (Amédéo et al., 2014). The stratotype of the Gault Clay defined in the Aube department consists of the Argiles Tégulines de Courcelles (82 m) overlain by the Marnes de Brienne (43

m). At ~23 Ma (Early Miocene), the Paris Basin was eroded and became almost similar to the present day. Nowadays the Gault Clay formation outcrops as a 8–10 km large and 80-km long band of terranes oriented NE-SW through the Aube department (Fig. 1a).

In the area we studied east of Brienne Le Chateau, Gault Clay is only represented by Tégulines Clay. The claystones consisted of the dominant clay fraction (47–72%) associated with a quartz-feldspar silty fraction (28–43%) and a carbonate fraction (0–22%) (Lerouge et al., 2018). Weathering of Tégulines Clay induced petrophysical, mineralogical and chemical changes (Lerouge et al., 2018).

2.2. Sampling and rock description

Samples were collected on three boreholes: AUB1010, AUB230 and AUB240, and a 5-m deep pit (TPH1-1) (Fig. 1b). The AUB1010 borehole, drilled in May 2015, crosscuts less than 1.9 m of surficial formations/ weathered clay that were lost during the drilling, and ~32 m of clay before attaining the Greensands. Seventeen core samples came from the Tégulines Clay. The AUB230 borehole, drilled in December 2017 near the TPH1-1 pit, crosscuts ~5 m of surficial formations and ~63 m of Tégulines Clay before attaining the Greensands. Eight samples came from surficial formations dug in TPH1-1 pit and 28 core samples from Tégulines Clay. The AUB240 borehole was drilled in May 2018. About 12 m of Brienne marls overlies ~70 m of Tégulines Clay and protect them from weathering (Fig. 1b). Twelve core samples came from the Brienne marls and 18 core samples from Tégulines Clay. All of these core samples were water-saturated.

The mineralogy and weathering profile of the AUB1010 borehole are detailed in Lerouge et al. (2018). The TPH1-1 pit and the AUB230 borehole were drilled in a cultivated cornfield in December 2017. The 0–0.3 m was a brownish sandy loam soil containing ~1.5 wt. % of organic carbon. In the TPH1-1 pit, the following 0.3–5 m were ochrous sandy loam formed of 61–70 wt.% quartz-feldspar sandy fraction and 21–32 wt.% of clay fraction that were crosscut by a grayish network associated with local black roots. Some detrital disseminated coarse quartz grains (up to 400 μm) are characteristic of these surficial formations. Surficial formations in the AUB230 borehole, ~10 m from the TPH1-1 pit, were very similar but the bottom part was poorer in coarse detrital quartz grains, and looked like in situ dismantled Tégulines Clay. The organic matter content of the 0–5 m zone was lower than 0.2 wt.%. The mineralogy of the clay in the AUB230 borehole was quite similar to the AUB1010 borehole, taking into account that the 34 m of the clay in the AUB1010 borehole corresponded to the last 34 m of the clay overlying Greensands aquifer (Lerouge et al., 2018) (Fig. 2). The organic matter content of Tégulines Clay is ~0.5 ± 0.1 wt.% (Debure et al., 2020; Duffy et al., 2014). The bottom of the clay formation is characterized by the highest clay content (70–72 wt.%), 27–29 wt.% of quartz – feldspar silty fraction and no carbonate. The overlying ~9–12 m corresponds to the clay-quartz rich unit (UAQ) and is characterized by high quartz – feldspar silty content (AUB1010: 41–43 wt.%; AUB230: 39–44 wt.%) and low carbonate contents of 0–9 wt.%. The overlying ~20 m crosscut in the AUB1010 borehole and ~35 m in the AUB230 borehole corresponded to the clay rich unit (UA unit), and were characterized by the highest clay content (AUB1010: 54–66 wt.%; AUB230: 50–53 wt.%), 4–8 wt.% of carbonates and lower quartz-feldspar silty content (32–41 wt.%). The overlying ~20–25 m crosscut only in the AUB230 borehole belonged to the carbonate-clay rich unit (UAC) with the highest calcite contents (16–27 wt.%) and the lowest quartz – feldspar silty contents (20–31 wt.%).

The oxidation profile developed in the clay from the AUB230 borehole was also very similar to that of the AUB1010 borehole, although the thickness in the two boreholes was very different. The top of the clay attained at 3.5–5 m below the ground surface consists of a plastic entirely oxidized claystone (57 wt.% of clay and 42 wt.% of quartz-feldspar), which progressively becomes greenish with a brown network associated with roots. Pyrite nodules and framboids entirely

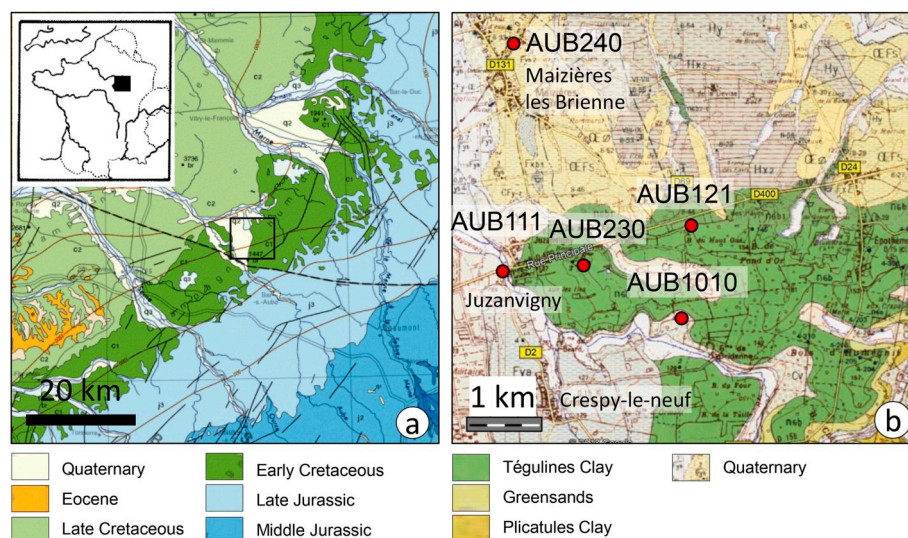


Fig. 1. (a) Geological map of the eastern part of the Paris basin and location of the studied area; (b) Location of the boreholes.

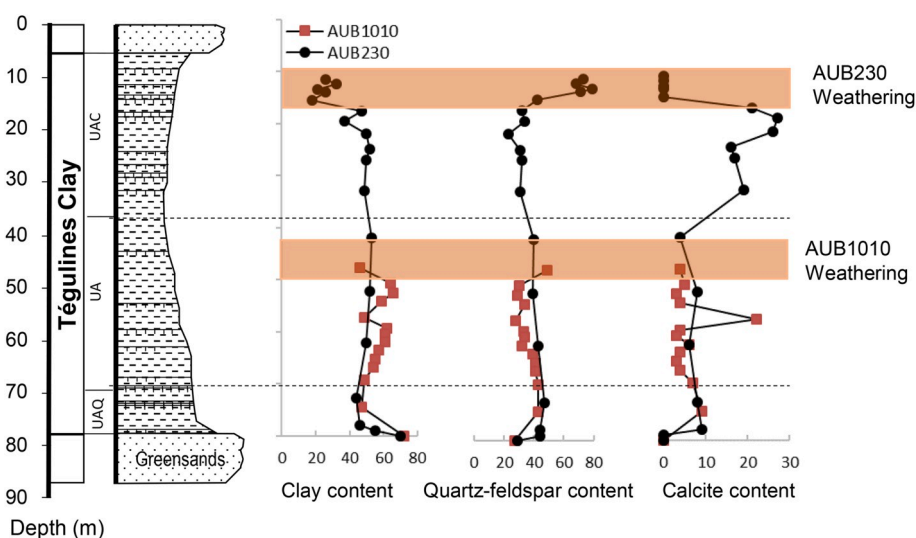


Fig. 2. Lithological log of Tégulines clay based on the AUB111 and AUB121 boreholes (Lerouge et al., 2018), and major mineralogy of Tégulines clay from the two boreholes AUB230 and AUB1010 and from the TPH1-1 pit with depth. The brownish zones indicate the surficial zones in which the weathering processes (reworked sediments/highly oxidized sediments) have significantly modified the bulk rock mineralogy.

broke down into gypsum associated with goethite. Carbonates are not detected by XRD but were still observed in thin sections (Fig. 3). The 5–11 m were plastic, yellowish green, and highly reactive; all the Fe-bearing minerals, including pyrite, glauconite were partially oxidized. Calcite gave evidence of partial dissolution, while gypsum and goethite precipitated (Fig. 3). Down to a depth of 20–25 m, Tégulines Clay is plastic, green with rare yellowish aggregates of glauconite that attest to tiny oxidation (Debure et al., 2018; Lerouge et al., 2018). Below 20–25 m, the reduced clay is dark green, nonplastic, nonfractured and unoxidized. Diagenetic assemblage including framboidal pyrite, calcite, glauconite and francolite supports reducing conditions.

3. Methods

3.1. Squeezing and pore water chemistry

Pore waters were extracted from clay samples by squeezing (Fernández et al., 2014), but using a modified method for collecting the squeezed pore waters under anoxic conditions. This method had already

been applied to clay core samples from the AUB1010 borehole (Lerouge et al., 2018). The core sample mass was measured before and after squeezing. The initial core sample masses ranged between 300 and 500 g. Extractions were carried out at pressures ranging between 5 and 60 MPa (Table 1) over 9 days. Approximately 20 mL of pore water was collected. Two successive pressures were applied to some samples to favor pore water extraction, as indicated in Table 1.

3.2. Core degassing protocol

3.2.1. Conditioning on the field

Core samples were immediately conditioned on the field after leaving the core sampler in order to minimize contact with atmosphere and to preserve in situ conditions of the clay-rocks, in particular the redox state. The first centimeters around the core were cut to avoid contamination of the clay by drill muds. The core samples were conditioned in glass jars of 0.5, 1 or 1.5 L under a He pressure of 600–700 10^{-3} bar after three short cycles of pumping and filling of He up to a pressure of 1.5 bar. The vacuum obtained with the pump corresponded to about 20–30

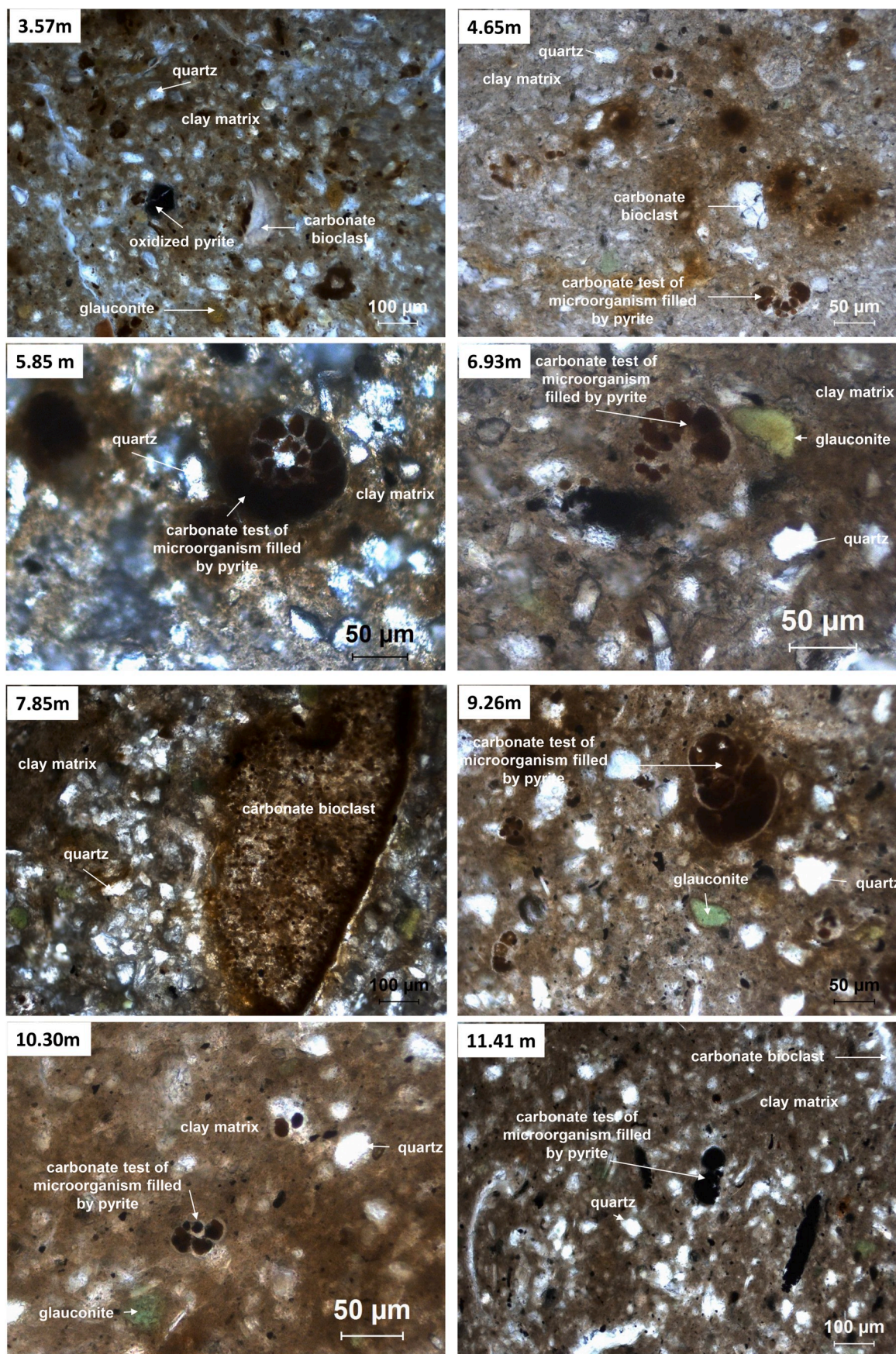


Fig. 3. Micrographs of the thin sections of téguline clay from the AUB230 borehole between 3.5 and 11.5 m in natural transmitted light providing evidence of the presence of carbonate bioclasts and pyrite oxidation down to 10.30 m.

Table 1

Chemical compositions of ground waters collected at 5.4 m in the TPH1-1 pit, and pore waters extracted by squeezing on four core samples from the TPH1-1 pit and of eleven samples from the AUB230 borehole. P were the successive pressure of extraction applied during the squeezing of the core sample.

	TPH1-1 pit					AUB230 borehole										
Depth (m)	0.3	1.7	2.4	4	5.4	5.9	7.9	11.4	15	21	30.4	41	50	61.3	66.3	68.4
P (MPa)	5	5,10	10	5	5	5	15	15, 30	10, 15	15	10, 20	40, 60	40	50	50, 60	40
pH	7.2	7.0	6.8	7.2	7.4	7.5	7.4	7.8	7.4	7.5	8.0	7.5	8.1	8.1	7.9	7.9
Alkalinity (meq/L)	1.4	0.9	<0.5	0.8		5.5	8.1	6.5	4.4	4.2	2.9	3.0	2.3	3.5	2.9	2.0
Cations (mmol/L)																
Na ⁺	0.4	0.9	0.9	0.6	0.6	5.4	8.5	7.0	3.9	3.3	2.6	2.8	2.2	2.1	4.3	1.6
K ⁺	0.03	0.03	0.04	0.04	0.02	0.4	3.3	0.8	0.7	0.7	0.6	0.4	0.3	0.2	0.6	0.2
Ca ²⁺	0.8	1.0	0.4	0.4	1.5	11.2	15.0	11.2	15.0	7.7	4.0	5.0	2.1	1.4	8.0	0.8
Mg ²⁺	0.2	0.4	0.2	0.1	0.2	4.9	8.0	7.0	9.9	6.8	3.9	4.5	1.5	1.3	7.8	0.7
Sr ²⁺				0.02		0.09	0.14	0.15	0.18	0.23	0.17	0.42	0.08	0.08	0.59	0.06
Al ³⁺				0.01												0.01
Si				0.24	0.23	0.43	0.57	0.27	0.16	0.17	0.21	0.20	0.17	0.15	0.18	0.13
Anions (mmol/L)																
Cl ⁻	0.2	0.7	0.9	0.5	0.4	7.8	12.6	14.8	12.7	6.8	2.8	1.5	2.0	1.9	1.1	1.1
SO ₄ ²⁻	0.3	0.5	0.1	0.1	0.2	9.8	18.7	15.6	20.8	12.5	5.4	8.7	2.1	1.4	15.6	1.0
NO ₃ ⁻	0.0	0.9	0.5		1.99		0.03				0.02		0.02	0.03		

10⁻³ bar. The pumping time was short to avoid clayrock desaturation. The three successive cycles of pumping and He fillings decreased the oxygen content in the gas phase (<5.10⁻⁷ mol of O₂). The samples were systematically weighed and ranged between 900 and 1000 g in a 1.5 L glass jar. The weight was proportionally adapted for other glass jars.

3.2.2. Gas monitoring

Glass jars were stored in a room at an almost constant temperature (~20 °C), and regularly monitored for total gas pressure (P_{total} expressed in bar) and concentrations of different gas species (CO₂, alkanes, oxygen and nitrogen) on a Varian star 3400 CX gas chromatograph over several months (at least 2 months). Oxygen and nitrogen gases were systematically measured to test the gas-tightness of the glass jars. Concentrations of gas species ($X_{\text{gas species}}$) are given in volume percent. The uncertainty on the concentrations of CO₂, alkanes, O₂ and N₂ in the gas phase was 3%. The detection limits for gas concentrations were 0.001% for CO₂, O₂ and N₂, and 0.0002% for alkanes. The uncertainty on the total pressure measured in the chromatograph was 3 . 10⁻³ bar. Data are firstly expressed in partial pressure of gas species ($P_{\text{gas species}}$) using Equation (1):

$$P_{\text{gas species}} = \frac{X_{\text{gas species}}}{100} \times P_{\text{total}} \quad (\text{eq 1})$$

To establish the degassing duration necessary for a steady state and improve the technique, the seventeen clay core samples from the

AUB1010 borehole of the 2015 drilling campaign were regularly monitored for CO₂ for more than 200 days in the laboratory. The P_{CO_2} attained a steady state at about 60 days of degassing in all the gas-tight glass jars (Fig. 4a). In five glass jars where P_{total} , P_{O_2} and P_{N_2} increased slowly toward atmospheric values, providing evidence of micro-leaks, the P_{CO_2} went on to increase slowly (Fig. 4b). Two monitorings carried out on two aliquots of AUB1010–13.45 m showed that the P_{CO_2} measured in a leaking glass jar was higher than that measured in a gas-tight jar (Fig. 4b). In this study, the values of P_{CO_2} measured at 60 days in gas-tight jars were considered as representative of the P_{CO_2} of the gas/solid/pore water steady state.

3.2.3. Carbon isotopic composition of CO₂

At the final stage of core degassing, an aliquot of gas of each sample was transferred into He-flushed Labco®-vials. The stable carbon isotopic composition of CO₂ ($\delta^{13}\text{C}_{\text{CO}_2}$) was analyzed with a continuous flow Thermo Finnigan Delta^{plus} XP isotope ratio mass spectrometer equipped with a GasBench II (Thermo Finnigan) for gas preparation and introduction. Isotopic compositions are reported in δ units relative to international standards, defined by: $\delta = (R_{\text{Sample}}/R_{\text{Standard}} - 1) \times 1000\%$, where R is the measured isotopic ratio in the sample and in the standard: Vienna Standard Mean Ocean Water (V-SMOW) for oxygen, Vienna Pee Dee Belemnite (VPDB) for carbon. Internal reproducibility was $\pm 0.2\%$ for oxygen and carbon; accuracy for $\delta^{13}\text{C}$ measurements with respect to VPDB standard is better than $\pm 0.5\%$.

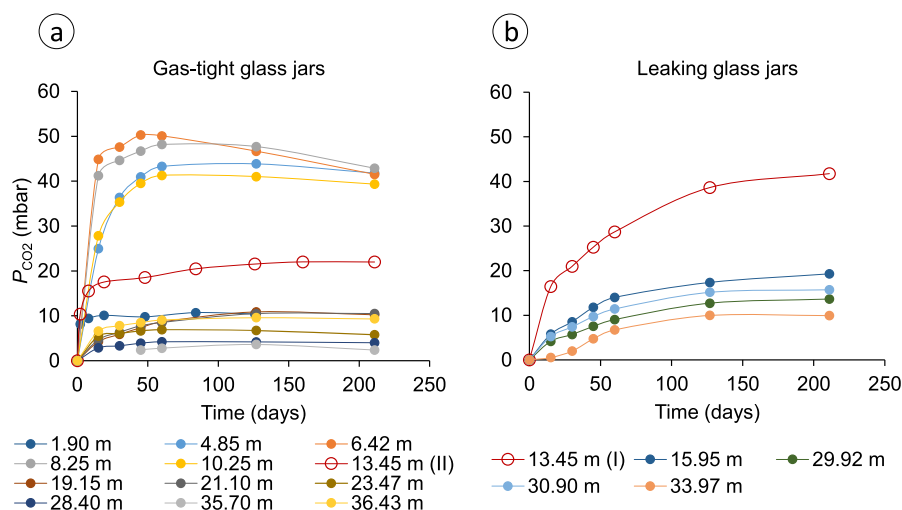


Fig. 4. P_{CO_2} monitoring (mbar) of core samples from the AUB1010 borehole. (a) gas-tight glass jars; (b) gas-leaking glass jars.

3.2.4. Successive core-degassing

Core degassing classically analyzes present-day dissolved gas. We now apply successive degassing stages to a same core sample to define the origin of the gas, and the processes that controlled their production. Reproducible concentrations of a gas species during successive degassing would indicate that the rock controls the processes of gas formation. Decreasing concentrations of a gas species during successive degassing would suggest that the gas species is present as a finite stock in the claystone.

At the end of the first monitoring and the sampling of the gas aliquot for the $\delta^{13}\text{C}_{\text{CO}_2}$ measurement, all the gas was pumped out of the glass jar, and the core sample was re-conditioned under a He pressure of 600–700 10^{-3} bar. The glass jar was again regularly monitored for total gas pressure (P_{total}) and concentrations of different gas species (CO_2 , alkanes, oxygen and nitrogen), according to the § 3.2.2. The reconditioning was applied two times to clay core samples from the AUB1010 and AUB230 boreholes.

3.3. Calculation of the concentrations of dissolved gas in pore waters

With the knowledge of all the parameters of the core degassing experiment, it is possible to estimate the initial concentrations of dissolved gas in pore waters (referred to as $[\text{gas species}]_0$) from the final measured partial pressures of gas ($P_{\text{gas species}}$). The experiment is a closed system in which the core sample degasses in an atmosphere of inert gas until obtaining steady state between gas, pore waters and solid (Fig. 5). In the initial system (0), core sample is water-saturated and the gas phase is only He. In the final system (f), gas species present in the gas phase are considered at equilibrium with gas dissolved in pore waters.

3.3.1. Oxygen and nitrogen

For gases such as oxygen and nitrogen, which are not controlled by the rock, the gas content in the rock represents a gas stock, which distributes between the gas phase (*gas*) and pore waters (*aq*) during the experiment. Consequently, for such gas species, it is possible to write the conservation equation of the species in the (gas + pore waters) system, as follows:

$$n_{\text{gas species}}(aq)_0 = n_{\text{gas species}}(gas)_f + n_{\text{gas species}}(aq)_f \quad (\text{eq 2})$$

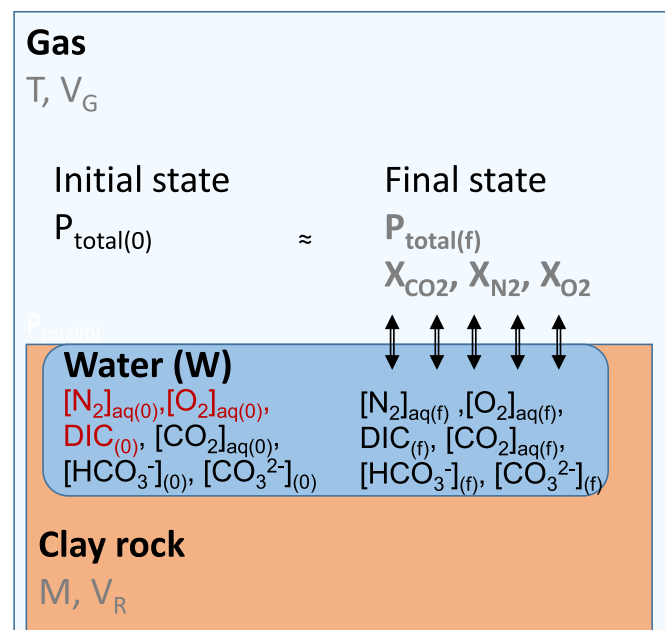


Fig. 5. Schema of the core degassing dispositive including all the parameters that are recorded.

where $n_{\text{gas species}}(gas)_f$ is the number of moles of the gas species at the end of the experiment, and $n_{\text{gas species}}(aq)_0$ and $n_{\text{gas species}}(aq)_f$ are the number of moles of the gas species dissolved in pore waters of the core sample at the beginning and at the end of the experiment, respectively.

The term $n_{\text{gas species}}(aq)$ depends on the sample mass (M), on the water content of the sample ($W\%$) and on the concentration of the gas species dissolved in pore waters ($[\text{gas species}]$) as follows:

$$n_{\text{gas species}}(aq) = \frac{M}{100} \times \frac{W}{1000} \times [\text{gas species}] \quad (\text{eq. 3})$$

By replacing $n_{\text{gas species}}(aq)$ in equation (2) with the above expression, $[\text{gas species}]_0$ can be expressed in function of $n_{\text{gas species}}(gas)_f$, M , W and $[\text{gas species}]_f$ as follows:

$$[\text{gas species}]_0 = n_{\text{gas species}}(gas)_f \left/ \left(\frac{M}{100} \times \frac{W}{1000} \right) \right. + [\text{gas species}]_f \quad (\text{eq. 4})$$

The term $n_{\text{gas species}}(gas)_f$ can be deduced from the ideal gas law applied to the partial pressure of the gas species $P_{\text{gas species}}$, and measured in the volume of gas (V_G) of the glass jar (Eqn 5):

$$n_{\text{gas species}}(gas)_f = P_{\text{gas species}} \times \frac{V_G}{R \times T} \quad (\text{eq. 5})$$

The $[\text{gas species}]_f$ can be deduced from the Henry's law as follows:

$$[\text{gas species}]_f = \frac{P_{\text{gas species}}}{K_{\text{H(gas species)}}} \quad (\text{eq. 6})$$

Replacing $n_{\text{gas species}}(gas)_f$ and $[\text{gas species}]_f$ in Equation (4) with the above expressions (Eqn 5 and 6), $[\text{gas species}]_0$ can finally be expressed as a function of $P_{\text{gas species}}$, V_G , M , W , and $K_{\text{H(gas species)}}$, which are known parameters:

$$[\text{gas species}]_0 = P_{\text{gas species}} \times \left\{ \left(\frac{V_G}{R \times T} \right) \left/ \left(\frac{M}{100} \times \frac{W}{1000} \right) \right. + \frac{1}{K_{\text{H(gas species)}}} \right\} \quad (\text{eq 7})$$

Nitrogen gas may be considered as an inert gas diffusing through Tégulines Clay. We consequently apply Equation (7) directly to estimate concentrations of dissolved N_2 in Tégulines pore waters. At 25 °C, $K_{\text{H}(\text{N}_2)}$ is 1639.34 (Schaap et al., 2001), and the term $1/K_{\text{H}(\text{N}_2)}$ is negligible.

Oxygen gas is a reactive gas diffusing through Tégulines Clay. For this reason, the concentrations of dissolved O_2 in Tégulines pore waters that may be calculated using Equation (7) need to be taken with caution, and probably represent minimum values. $K_{\text{H}(\text{O}_2)}$ is 769.23 at 25 °C (Schaap et al., 2001), and $1/K_{\text{H}(\text{O}_2)}$ is negligible, as is the case for nitrogen gas.

3.3.2. Dissolved inorganic carbon (DIC)

Contrary to O_2 and N_2 gas, for which gas pressure is directly related to dissolved gas concentration by the Henry law, the CO_2 partial pressure is related to dissolved CO_2 by the Henry law, but total dissolved inorganic carbon is distributed among three species $\text{CO}_2(aq)$, HCO_3^- and CO_3^{2-} . Consequently, calculations need to take into account all the carbonate species dissolved in pore waters as the total dissolved carbonate content (DIC) is defined by Equation (8) :

$$\text{DIC} = [\text{CO}_2(aq)] + [\text{HCO}_3^-] + [\text{CO}_3^{2-}] \quad (\text{eq 8})$$

At equilibrium, $[\text{HCO}_3^-]$ and $[\text{CO}_3^{2-}]$ can be expressed in term of $[\text{CO}_2(aq)]$, K_1 , K_2 and $[\text{H}^+]$, K_1 being the reaction constant for $\text{CO}_2(aq) = \text{H}^+ + \text{HCO}_3^-$ and K_2 being the reaction constant for $\text{HCO}_3^- = \text{H}^+ + \text{CO}_3^{2-}$ (Giffaut et al., 2014):

$$\text{DIC} = [\text{CO}_2(aq)] \times (1 + K_1 \times [\text{H}^+] + K_1 \times K_2 \times [\text{H}^+]^2) \quad (\text{eq 9})$$

Taking into account all the carbonate species dissolved in pore waters, the conservative Equation (2) can be applied to the total amount of

moles of carbonates dissolved in pore waters ($n_{\text{DIC}}(aq)$) and CO_2 gas ($n_{\text{CO}_2}(\text{gas})$) during experiments, as follows (Eqn 10):

$$n_{\text{DIC}}(aq)_0 = n_{\text{CO}_2}(\text{gas})_f + n_{\text{DIC}}(aq)_f \quad (\text{eq 10})$$

By replacing $n_{\text{DIC}}(aq)$ by their expressions given in equation (3), total dissolved inorganic carbon content DIC_0 can be expressed as a function of $n_{\text{gas species}}(\text{gas})_f$, M , W and $[\text{gas species}]_f$:

$$\text{DIC}_0 = n_{\text{CO}_2}(\text{gas})_f \left/ \left(\frac{M}{100} \times \frac{W}{1000} \right) \right. + \text{DIC}_f \quad (\text{eq 11})$$

According to the ideal gas law, $n_{\text{CO}_2}(\text{gas})_f = P_{\text{CO}_2} \times \frac{V_G}{R \times T}$

According to equation (9) applied to final state of the experiment,

$$\text{DIC}_f = [\text{CO}_2(aq)]_f \times (1 + K_1 \times [\text{H}^+] + K_1 \times K_2 \times [\text{H}^+]^2)$$

$$\text{DIC}_f = P_{\text{CO}_2} / K_{\text{H}(\text{CO}_2)} \times (1 + K_1 \times [\text{H}^+] + K_1 \times K_2 \times [\text{H}^+]^2),$$

$$\text{with } [\text{CO}_2(aq)]_f = P_{\text{CO}_2} / K_{\text{H}(\text{CO}_2)}$$

Replacing $n_{\text{CO}_2}(\text{gas})_f$ and DIC_f in Equation (11) by the above expressions, DIC_0 can finally be expressed as a function of P_{CO_2} , V_G , M , W , and $K_{\text{H}(\text{CO}_2)}$, which are known parameters (Eqn 12):

$$\text{DIC}_0 = P_{\text{CO}_2} \times \left\{ \left(\frac{V_G}{R \times T} \right) \left/ \left(\frac{M}{100} \times \frac{W}{1000} \right) \right. + \frac{(1 + K_1 \times [\text{H}^+] + K_1 \times K_2 \times [\text{H}^+]^2)}{K_{\text{H}(\text{CO}_2)}} \right\} \quad (\text{eq 12})$$

For CO_2 , contrary to O_2 and N_2 , the term $\frac{(1 + K_1 \times [\text{H}^+] + K_1 \times K_2 \times [\text{H}^+]^2)}{K_{\text{H}(\text{CO}_2)}}$ is low but cannot be neglected. $[\text{H}^+]$ is deduced from the pH values of pore waters extracted by squeezing. The equilibrium constants pK_1 and pK_2 are 6.37 and 10.33 at 25 °C (Giffaut et al., 2014).

4. Results

4.1. Pore water chemistry

Pore waters of four samples of surficial formation from the TPH1-1 pit and of eleven clay core samples from the AUB230 borehole were extracted by squeezing. Natural ground waters from the TPH1-1 were also collected at 5.4 m deep. The chemistry of the pore waters was given in Table 1.

The pore waters extracted from surficial formations and natural ground waters at 5.4 m in the TPH1-1 pit have neutral pH values of ~7.2–7.4, and low alkalinities of 0.57 meq/L. It is noteworthy that pore waters extracted by squeezing and natural pore waters in surficial formations have consistent chemical compositions. The clay's pore waters have pH values ranging from 7.4 to 8.2, and alkalinity ranging from 1.2 to 9.9 meq/L. Pore waters in samples from the lower part of the clay formation are characterized by the lowest alkalinity values and may be classified as Ca-sulfate type waters. Pore waters in weathered samples of the upper part of the clay formation are characterized by increasing alkalinity and evolve to Ca–Mg-sulfate type waters toward the surface.

4.2. Gas monitoring

We applied a core-degassing protocol to the eight samples of surficial formation from the 5-m deep TPH1-1 pit, the twelve samples of Brienne marls from the AUB240 borehole, and the sixty-three clay core samples from the three AUB240 (18 samples), AUB230 (28 samples) and AUB1010 (17 samples) boreholes. We applied two other successive core degassing procedures on the clay core samples from the AUB230 borehole and the AUB1010 borehole, in order to define the process of gas formation. All the gas measurements were expressed as concentrations of dissolved gas in mmol/L of pore water (supplementary data; Fig. 6). The P_{CO_2} were also given for comparison with literature data

(supplementary data).

4.2.1. Gas monitoring of reduced Tégulines Clay: AUB240 reference borehole

About 12 m of Brienne marls overly Tégulines Clay in borehole AUB240 and protect them from weathering. Core degassing of overlying Brienne marls have CO_2 concentrations ranging between 1.2 and 4.3 mmol/L PW. The highest values are measured in the upper part of the Brienne marls in contact with alluvium. The O_2 concentrations vary a lot with values up to 0.39 mmol/L PW, and N_2 concentrations range between 0.7 and 7.7 mmol/L PW.

The CO_2 , O_2 and N_2 profiles of reduced Tégulines Clay with depth are almost flat. A reference-average CO_2 concentration calculated between the top of the clay at 20 m and the bottom at 90 m is 1.5 ± 0.5 mmol/L PW. The O_2 concentrations were generally below the detection limit except for four samples, whereas the average N_2 concentration was 1.8 ± 1.0 mmol/L PW. The CH_4 concentrations ranged between $1.15 \cdot 10^{-3}$ and $4.3 \cdot 10^{-3}$ mmol/L PW. The highest values were measured in the middle of the formation.

4.2.2. Gas monitoring of weathered Tégulines Clay: AUB1010 and AUB230 boreholes

4.2.2.1. AUB230 borehole. The 5-m deep TPH1-1 pit and the AUB230 borehole crosscut ~5 m of surficial formations consisting of soil and sandy loam, and ~63 m of weathered Tégulines Clay before attaining the Greensands. The soil sample (TPH1-1 0–30 cm) directly in contact with the atmosphere degassed a lot of CO_2 (11.5 mmol CO_2 /kg of soil), and a significant amount of CH_4 ($1.9 \cdot 10^{-1}$ mmol/L PW). The N_2 concentration was high (10.6 mmol/L PW), whereas the O_2 concentration was very low (0.04 mmol/LPW). Samples of underlying surficial formations down to 5 m degassed less CO_2 than soil (1.4–2.7 mmol/L PW). The O_2 and N_2 concentrations varied a lot with values up to 2.1 and 11.7 mmol/L PW, respectively. Methane was not detected. The CO_2 , O_2 and N_2 profiles of weathered Tégulines Clay with depth are curvilinear (Fig. 6). The O_2 concentrations reached up to 0.9 mmol/L PW in the 5–10 m zone and were close to the detection limit below 10 m down to 68 m. The N_2 profile was almost flat with values ranging between 1.4 and 4.7 mmol/L; increased N_2 concentrations was however observed at ~25 m (up to 6.9 mmol/L PW). The CO_2 concentrations significantly increased up to 8.5 mmol/L PW in the 5–15 m zone, in relation with the increase of the O_2 concentrations. Below ~20 m, the CO_2 concentrations ranged between 0.5 and 3.3 mmol/L PW, with an average value of 1.6 ± 0.9 mmol/L PW. The CH_4 concentrations ranged between $4.1 \cdot 10^{-4}$ and $\sim 3.5 \cdot 10^{-3}$ mmol/L PW with the highest value measured in the middle of the formation.

4.2.2.2. AUB1010 borehole. Tégulines Clay is very close to the surface in the AUB1010 borehole. The CO_2 , O_2 and N_2 profiles of the weathered clay with depth are also curvilinear (Fig. 6). The O_2 concentrations reached up to 1.8 mmol/L PW in the 1.9–10 m zone and were close to the detection limit below 10 m down to 34 m, whereas the N_2 concentrations varied a lot, ranging between 2.3 and 14.2 mmol/L PW. The CO_2 concentrations significantly increased up to 8.6 mmol/L PW in the 1.9–15 m zone, in relation with the increase of the O_2 concentrations. Below ~20 m, the CO_2 concentrations ranged between 1.2 and 2.8 mmol/L PW, with an average value of 1.7 ± 0.8 mmol/L. The CH_4 concentrations were lower than $9.6 \cdot 10^{-4}$ mmol/L PW, except a value of $1.5 \cdot 10^{-3}$ mmol/L PW at interface with Greensands.

4.2.2.3. Second and third gas degassing. The CO_2 profiles of the second degassing of core samples from boreholes AUB1010 and AUB230 have the same shape as the CO_2 profiles from the first degassing (Fig. 7). However, the CO_2 values measured in the upper part (<15 m) were lower than that of the first degassing at the same depth (Fig. 7). The CO_2

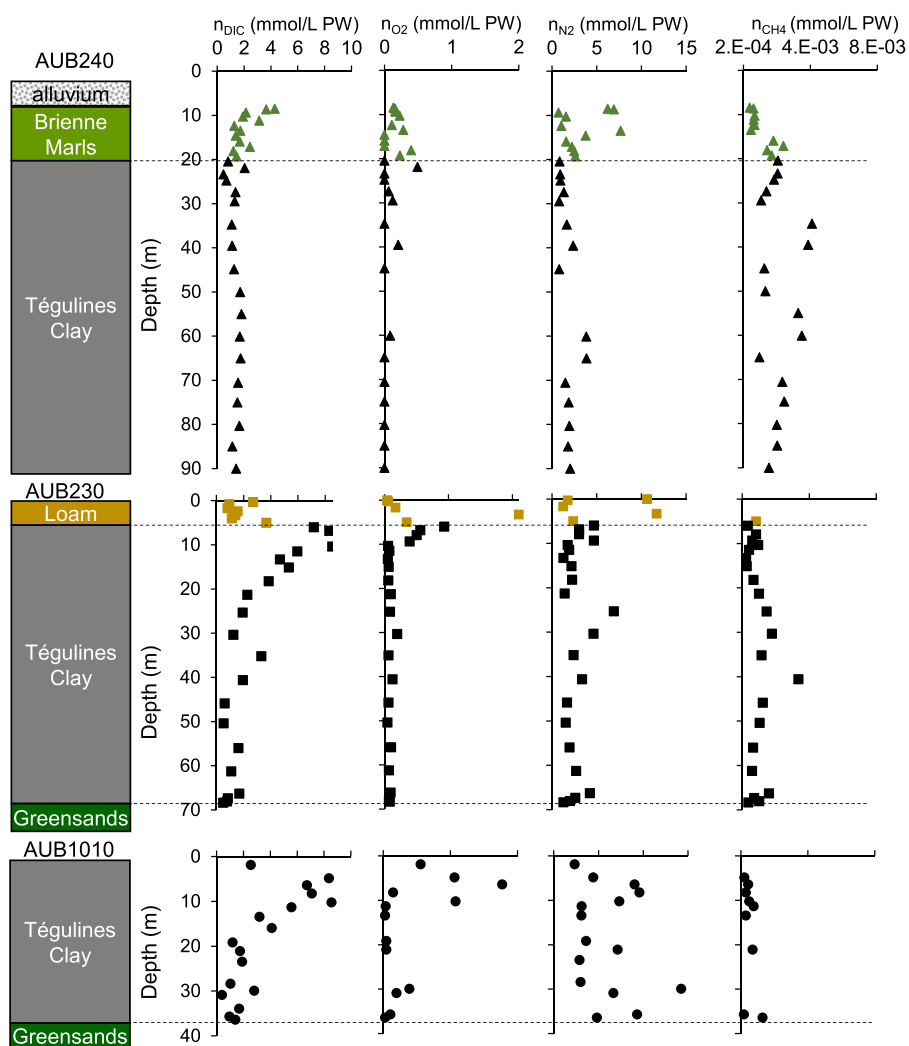


Fig. 6. Gas concentrations (CO_2 , CH_4 , O_2 and N_2) of samples from AUB1010, AUB230 and AUB240 boreholes with depth. A schematic log is given for each borehole to define the interfaces of Téguline Clay with surficial formations (loam) and Greensands. Data are given in mmol/L of pore water (PW). Black symbols represent Tégulines Clay data, green symbols Brienne marl data and yellow symbols loam data. (For interpretation of the references to colour in this figure legend, the reader is referred to the Web version of this article.)

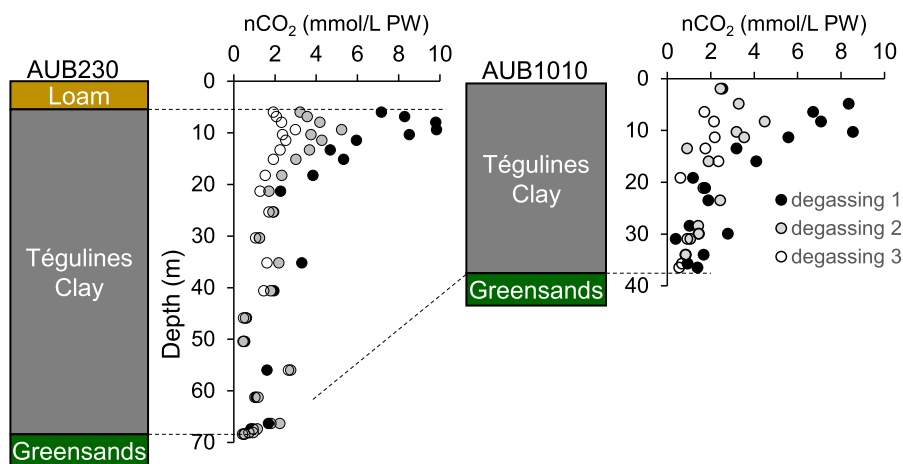


Fig. 7. CO_2 profiles with depth established for the three successive degassings of core samples from the AUB1010 and AUB230 boreholes. A schematic log is given for each borehole to define the interfaces of Téguline Clay with surficial formations (loams) and Greensands. Data are given in mmol/L of pore water (PW).

profile of the third degassing was quite flat, with an average CO_2 concentration of 1.4 ± 0.7 mmol/L PW for the AUB1010 borehole and of 1.6 ± 0.7 mmol/L PW for the AUB230 borehole.

Oxygen, nitrogen and methane concentrations measured in gas during the second and third degassings were near or below the detection limit of the technique.

4.3. Carbon isotopic composition of CO_2

The $\delta^{13}\text{C}_{\text{CO}_2}$ largely ranged between -25.5 and -7.7 ‰ PDB. The profiles of $\delta^{13}\text{C}_{\text{CO}_2}$ with depth were different in the three boreholes (Fig. 8). The $\delta^{13}\text{C}_{\text{CO}_2}$ profile of reduced Tégulines Clay from the AUB240 borehole with depth was almost flat, with values ranging between -12.0 and -7.9 ‰ PDB. The highest values were measured at the top in contact with Brienne marls. The $\delta^{13}\text{C}_{\text{CO}_2}$ of Brienne marls are in the same range as Tégulines Clay.

The profiles of $\delta^{13}\text{C}_{\text{CO}_2}$ of the AUB1010 and AUB230 boreholes with depth are curvilinear. The $\delta^{13}\text{C}_{\text{CO}_2}$ of the clay from the AUB230 and AUB1010 boreholes ranged between -19.5 and -10.5 ‰ PDB, and between -19.8 and -12.5 ‰ PDB, respectively. The highest values were measured at ~ 20 – 22 m for the AUB1010 borehole (-12.9 to -12.5 ‰ PDB), and between 15 and 40 m for the AUB230 borehole (-11.8 to -10.3 ‰ PDB). The lowest values were measured toward the top and the bottom of the formation.

The surficial formations overlying the clay in the AUB230 borehole had the lowest values: -25.5 ‰ VPDB for the soil sample (TPH1-1 0–30 cm) in contact with atmosphere, and -21 ‰ VPDB for underlying sandy loam.

5. Discussion

5.1. Dissolved gas contents of reduced Téguline Clay pore waters – Comparison with other reduced-marine clays

The most representative, well-preserved reduced Tégulines Clay from the AUB240 borehole between 20 and 90 m deep is characterized by O_2 concentrations below the detection limit and an average P_{CO_2} of $4.1 \pm 0.9 \cdot 10^{-3}$ bar. These results are in the range of P_{CO_2} compiled by Araújo Reis and Brantley (2019) for sedimentary confined aquifers (1–100 mbar at 25 °C), and of P_{CO_2} values of other marine reduced formations (Gaucher et al., 2009, 2010; Lerouge et al., 2015; Tremosa et al., 2012; Wersin et al., 2016). The P_{CO_2} profile with depth is almost flat. This can be a good indication of internal control of this parameter by the mineralogy as its nature is constant throughout the formation.

The highest $\delta^{13}\text{C}_{\text{CO}_2}$ (-10.4 to -7.9 ‰) are consistent with $\delta^{13}\text{C}_{\text{CO}_2}$ calculated at equilibrium with calcite in Tégulines Clay, where the $\delta^{13}\text{C}$

ranges between 0.4 and 2.9‰ (Lerouge et al., 2018), and carbon isotopic fractionation between calcite and $\text{CO}_2(\text{g})$ of 10.5‰ at 20 °C (Deines et al., 1974; Mook et al., 1974). They also agree well with values measured in other reduced clay formations, and confirm that degassed CO_2 is controlled by carbonates in the mineral assemblage and not by degradation of organic matter or diffusion of gas coming from other geological formations (Gaucher et al., 2006, 2010; Girard et al., 2005; Tremosa et al., 2012).

5.2. Influence of weathering on chemistry and dissolved gas contents of Téguline Clay pore waters

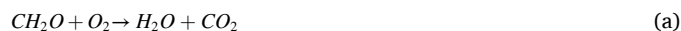
Present-day pore waters from Tégulines Clay outcrops have a complex history resulting from their past interactions with external waters coming from overlying Cretaceous chalk, and from their current interactions with percolating meteoric waters and ground waters of the underlying Greensands aquifer. Tégulines Clay is a marine-clay formation that originally evolved in reducing conditions. After 23 Ma of erosion in the Paris Basin, present-day Tégulines clay outcrops or is overlaid by soils and a few meters of surficial formations in the studied area. The bottom of the Tégulines Clay is in contact with the Greensands aquifer, whose water recharge is located less than 10 km southeast.

Below we discuss the nature of the external fluids and modifications to the chemistry and dissolved gas (O_2 , N_2 and CO_2) concentrations in Tégulines Clay pore waters through the weathering profile.

5.2.1. Surficial fluids through soil and surficial formations

At surface and down to the top of the clay (example of the AUB230 borehole), pore waters are infiltrating meteoric waters, which interact with mineral assemblage in carbonate-free soil and surficial formations. These waters analyzed by squeezing and natural ground waters collected in the pit at ~ 5.4 m were much-diluted $\text{Ca} - \text{HCO}_3^-$ type waters.

The pore water at 0–30 cm shows the highest alkalinity: ~ 1.4 meq/L. The $\delta^{13}\text{C}_{\text{CO}_2}$ of soil (-25.5 ‰) indicates that the CO_2 derived from organic matter degradation. During the monitoring of soil degassing, the CO_2 concentration rapidly increased, whereas O_2 concentration was low (supplementary data). These data indicate that CO_2 results from the degradation of organic matter, according to the respiration reaction (a):



Between 0.3 and 5 m, the DIC of surficial formations were less than 0.9 meq/L. The significant DIC difference between soil and surficial formations can be interpreted in different ways:

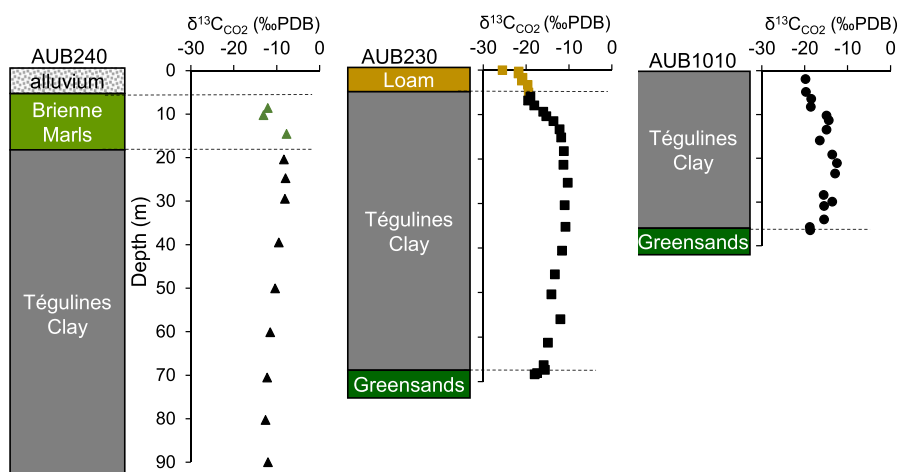


Fig. 8. $\delta^{13}\text{C}_{\text{CO}_2}$ of samples from AUB1010, AUB230 and AUB240 boreholes with depth. A schematic log is given for each borehole to define the interfaces of Téguline Clay with surficial formations (loam) and Greensands. Data are given in δ permil relative to the PDB standard. Black symbols represent Tégulines Clay data, green symbols Brienne marl data and yellow symbols loam data. (For interpretation of the references to colour in this figure legend, the reader is referred to the Web version of this article.)

- 1) CO₂ was produced internally by soil and surficial formations, and DIC differences were due to lower organic matter content in surficial formation (0.2 wt.%) than in soil (1.5 wt.% in soil);
- 2) CO₂ was produced internally by soil and surficial formations, and DIC differences were due to lower oxygen support in surficial pore waters than in soil; the diffusion rate of dissolved oxygen was four times lower than that of oxygen gas (Bolton et al., 2006);
- 3) CO₂ produced by organic matter degradation migrated into surficial formation.

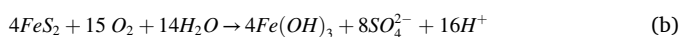
The presence of abnormal high O₂ and N₂ concentrations in surficial formations (higher than dissolved gas solubility) indicates the presence of trapped atmosphere bubbles. That also strongly suggests that organic matter is not degraded much in the surficial formation. The flat CO₂ profile in the surficial formation would rather indicate advective transport of CO₂ produced by soil through surficial formation toward Tégulines Clay.

5.2.2. Weathered Tégulines Clay

Pore waters at the top of the Tégulines Clay have a significantly higher ionic strength than pore waters infiltrated from surficial formations and well-preserved, reduced Tégulines Clay pore waters, due to higher alkalinity, and calcium, chloride and sulfate contents. Core degassing also provided evidence of the highest DIC (up to ~9 mmol/L PW), and dissolved O₂ and N₂ concentrations. Some O₂ and N₂ concentration values were higher than gas solubility; that could be due to uncertainties on the water content, desaturation of the sample, or air bubbles trapped by the core samples.

The highest chemical changes were observed from the top of the formation down to ~10 m, corresponding to the highly reactive transition zone (AUB1010: Lerouge et al. (2018); AUB230: this study). These changes in pore water chemistry have already been described in other case studies (Brantley et al., 2013; Hendry and Wassenaar, 2000; Jin and Brantley, 2011; Tuttle and Breit, 2009; Tuttle et al., 2009) and predicted by reactive-transport modelling of weathering in clay aquitard (Heidari et al., 2017; Jin et al., 2010; Kim and Lee, 2009).

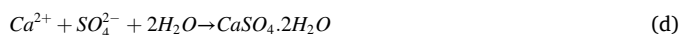
Chemical variations in the pore water, including high alkalinity and DIC, result from interactions between oxygenated surficial waters and mineral assemblage of the reduced clay. The O₂ concentrations recorded in this zone attest to the presence of O₂ that drives oxidative weathering of pyrite, organic matter and other Fe²⁺ bearing minerals including clay minerals (illite, illite-smectite mixed layers, chlorite, glauconite), carbonates (ankerite) and magnetite (Brantley et al., 2013; Debure et al., 2020; Duffy et al., 2014; Lerouge et al., 2018). The oxidation of pyrite in the presence of water is a source of protons according to reaction (b) that contributes to carbonate dissolution and DIC increase (Lebedeva et al., 2007; Torres et al., 2014):



The increase of protons induces calcite dissolution according to reaction (c):



Iron hydroxides and gypsum are secondary minerals formed from reactions (b) and (d), respectively:



Below 10–11 m down to ~15–18 m, the DIC, dissolved O₂ and N₂ concentrations, and cation and anion concentrations rapidly decreased to reach a relatively homogeneous reduced clay composition. The O₂ concentration became close or below the detection limit in agreement with reducing conditions.

At the bottom of the Tégulines Clay in contact with Greensands, pore waters had a significantly lower ionic strength than pore waters in preserved clay, providing exchanges between Tégulines clay and the

Greensands aquifer. The low ionic strength of pore waters was related to slightly lower DIC than reference Tégulines Clay. Claystone does not show any evidence of weathering, but calcite is absent.

5.2.3. Origin of dissolved inorganic carbon in weathered Tégulines Clay

The major reactions increasing the DIC in weathered Tégulines Clay are the dissolution of carbonates present in the claystone and the degradation of organic matter from external and internal sources. The wider δ¹³C_{CO2} range (−19.8 to −10.5‰) of the weathered clay than for reduced clay internally controlled by calcite (δ¹³C_{CO2-calcite} ~ −10.4 to −7.9‰ PDB) is consistent with mixing between the CO₂ component internally controlled by calcite, and a second CO₂ component due to degradation of organic matter, whose δ¹³C_{CO2-organic matter} is assumed ~ −25.5‰ PDB. From the δ¹³C_{CO2} of each clay sample, we estimate the contribution of these components (X_{organic matter} and X_{calcite}) in percent for the three boreholes (Fig. 9). The profiles of organic contribution are similar in the AUB1010 and AUB230 boreholes and provide evidence that degradation of organic matter is the major source of CO₂ in calcite-free surficial formations (X_{organic matter} ~60–80%), at the top of the clay down to ~8–9 m (X_{organic matter} ~32–60%), and toward the interface with Greensands (X_{organic matter} up to 60%). The depth of about 10 m corresponds approximatively to the depth of the root network observed in boreholes.

The contributions given in percent may be used to estimate the DIC associated to these contributions:

$$DIC_{\text{calcite}} = X_{\text{calcite}} \times DIC \quad \text{and} \quad DIC_{\text{organic matter}} = X_{\text{organic matter}} \times DIC$$

From the top of the clay to ~10 m for AUB230 and AUB1010, the DIC_{calcite} increased from 1 to 2 to 6.5 mmol/L, and then decreased to ~1–2 mmol/L at 20–25 m for AUB 230 and at 16 m for AUB1010. The DIC_{calcite} in the weathered clay was higher than the average DIC value measured in the reduced clay, which is attributed to calcite equilibrium in the reduced system (1.5 ± 0.5 mmol/L PW referred to as DIC_{calcite 0}). That confirms the displacement of the carbonate system (DIC_{calcite} dissolution) with pyrite oxidation and decreasing pH (Table 2). According to the reaction (c), 1 mole of CO₂ and 1 mole of Ca are produced by dissolution of 1 mol of CaCO₃. The DIC_{calcite} dissolution partially explains the Ca concentration increase in pore waters, but Ca concentration is also controlled by Ca-bearing mineral precipitation such as gypsum and the clay exchanger (Lerouge et al., 2018).

The DIC_{calcite} dissolution also can be expressed in millimoles of dissolved calcite per 100 g of rock, using the water and carbonate contents of the rock (Table 2). Even though CO₂ degassing reveals the effects of weathering on the clay, the calculated percentages of calcite dissolution to explain CO₂ degassing data remain small (<0.3 mmol of calcite per 100 g of rock) in the highly reactive transition zone. They are however higher in the weathered clay from the AUB1010 than from the AUB230 borehole. That is consistent with a higher intensity of clay weathering in the AUB1010 borehole, suggested by decreasing methane, and increasing oxygen and nitrogen degassing. It is noteworthy that our calculations correspond to a measurement at a time t of a reactive system, i.e. in situ reactivity and diffusion of pore waters through the formation. The diffusion rate of oxygen dissolved in pore waters is so slow that we assume minerals and the system were at a steady state (pseudo-equilibrium) at a time t.

On the other side, at the bottom of the clay at ~34 m in the AUB1010 borehole and at ~68 m in the AUB230, the DIC was lower than in preserved reduced Tégulines and δ¹³C_{CO2} was ~ −18‰, suggesting a dilution or isotopic exchange of CO₂ internally controlled by calcite with Greensands waters poor in CO₂ of organic origin. The profile of the δ¹³C_{CO2} in the lower part of the clay suggests progressive diffusion of CO₂ of organic origin through the clay formation up to ~30–40 m in the AUB230 borehole and ~20–25 m in the AUB1010 borehole.

Assuming contemporaneous weathering progressions at the top and the bottom of Tégulines clay in the AUB230 and AUB1010 boreholes, the lower thickness of the clay formation in the AUB1010 borehole and

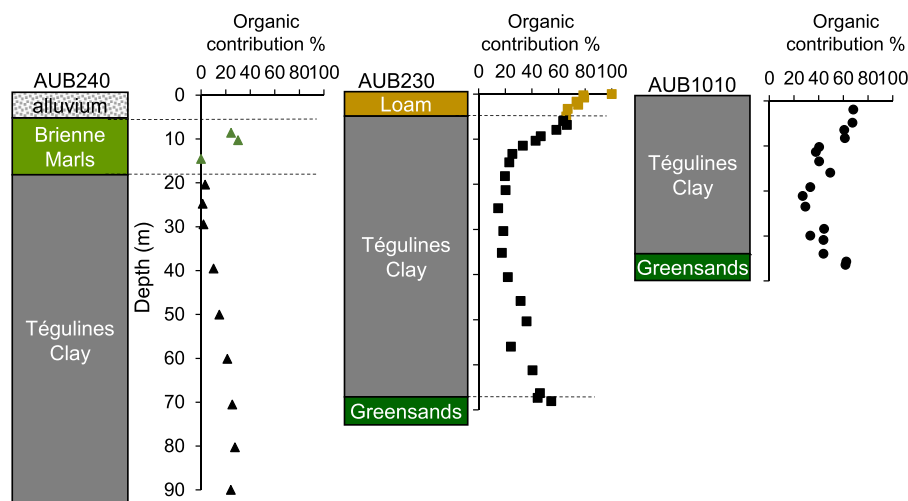


Fig. 9. Organic contribution (%) calculated on the base of a mixing between an organic CO₂ endmember (−25‰ PDB) and a calcite equilibrium-derived CO₂ endmember (−7.7‰ PDB).

Table 2

AUB1010 and AUB230 boreholes - DIC, δ¹³C_{CO₂}, concentrations of CO₂ attributed to degradation of organic matter (DIC_{organic matter}), to total calcite (DIC_{calcite}) calculated on the basis of a mixing between an organic CO₂ end-member (−27.4 ± 1.9‰ PDB) (DIC_{organic matter}) and a calcite equilibrium-derived CO₂ end-member (−9.0 ± 1.3‰ PDB) and to calcite dissolution (DIC_{calcite dissolution}) calculated by DIC_{calcite} - DIC_{calcite 0} (1.5 ± 0.5 mmol/L PW), water content of the sample, conversion of DIC_{calcite dissolution} in mmol/100 g of rock, calcite content of the sample and estimation of the percent of calcite dissolution due to calcite system displacement.

	DIC	δ ¹³ C	DIC	DIC	σ	DIC	σ	water content	DIC	Calcite content	calcite diss.
	mmol/L	‰	organic matter	calcite		calcite dissolution		%	calcite dissolution	mol/100 g	%
			mmol/L			mmol/L			mmol/100 g		
AUB230											
0.0	65.7	−25.5	65.7	0.0	−	−	−	20.5	−	0.00	−
0.3	3.1	−21.7	2.4	0.7	0.08	−	−	18.4	−	0.00	−
0.8	1.1	−21.8	0.9	0.3	0.03	−	−	17.8	−	0.00	−
1.7	0.9	−20.8	0.7	0.3	0.03	−	−	22.7	−	0.00	−
2.4	1.8	−21.0	1.3	0.5	0.06	−	−	15.5	−	0.00	−
3.3	1.6	−19.6	1.0	0.6	0.07	−	−	16.3	−	0.00	−
5.0	4.2	−19.4	2.6	1.6	0.18	−	−	18.5	−	below dl	−
6.0	8.3	−19.0	5.0	3.3	0.4	2.2	1.1	19.0	0.04	0.21	0.02
6.8	9.7	−19.5	6.1	3.5	0.4	2.5	1.2	18.2	0.05	0.21	0.02
8.0	10.9	−18.1	6.0	5.0	0.6	3.9	1.3	14.4	0.06	0.27	0.02
9.4	11.4	−16.0	4.8	6.6	0.8	5.0	1.3	18.5	0.09	0.27	0.03
10.4	9.9	−15.3	3.7	6.2	0.7	4.5	1.2	16.6	0.08	0.26	0.03
11.5	6.7	−13.6	1.8	4.9	0.6	3.4	0.9	16.5	0.06	0.26	0.02
13.3	5.3	−12.2	1.0	4.4	0.5	2.8	0.8	16.9	0.05	0.26	0.02
15.1	6.0	−11.8	1.0	5.0	0.6	3.5	0.9	15.9	0.06	0.26	0.02
18.2	4.3	−11.2	0.5	3.7	0.4	2.3	0.7	13.2	0.03	0.26	0.01
21.3	2.6	−11.3	0.3	2.2	0.3	0.9	0.6	15.6	0.01	0.26	0.01
25.3	2.2	−10.3	0.2	2.0	0.2	0.7	0.6	15.6	0.01	0.26	0.00
AUB1010											
1.9	2.6	−19.8	1.9	1.0	0.1	0.4	0.4	18.9	0.01	0.05	0.01
4.9	8.8	−19.7	6.3	3.5	0.4	2.6	1.3	24.0	0.06	0.05	0.12
6.4	8.1	−18.5	4.6	3.5	0.4	2.8	1.2	23.0	0.06	0.03	0.22
8.3	8.0	−18.6	4.9	3.6	0.4	2.7	1.2	19.6	0.05	0.04	0.13
10.3	9.0	−14.9	3.5	6.4	0.7	5.0	1.2	17.6	0.09	0.06	0.15
11.3	5.6	−14.4	2.1	4.5	0.5	2.8	1.0	18.6	0.05	0.04	0.13
13.5	3.2	−14.9	1.4	2.5	0.3	1.1	0.8	23.5	0.03	0.03	0.08
16.0	2.5	−16.5	2.1	2.6	0.3	0.5	0.5	16.5	0.01	0.06	0.02
19.2	1.2	−13.6	0.4	1.1	0.1	0.2	0.2	20.1	0.00	0.03	0.01
21.1	1.7	−12.5	0.4	1.7	0.2	0.5	0.5	15.5	0.01	0.04	0.02

decompaction processes might explain the higher weathering intensity in AUB1010 borehole.

5.3. Modeling approach

The distribution of DIC and major ions (Ca, Mg, Cl, SO₄²⁻) with depth showed that the main geochemical reactions occur in the soil zone (organic matter degradation), the highly reactive and 0–10 m oxidized

clay zone (pyrite oxidation and calcite dissolution), and in a lower proportion at the interface with aquifer waters of underlying Greensands. The solute profiles in the unoxidized clay are consequently the result of downward diffusion from pore waters of the oxidized clay and of upward diffusion from aquifer waters of underlying Greensands. Even though chloride is generally considered as a natural conservative tracer, chloride also shows a curvilinear profile relatively well-correlated with DIC, Ca, Mg and SO₄²⁻ profiles. These ion concentrations combined with

previous oxygen and hydrogen isotopes of clay pore waters in the first 10 m of the AUB1010 borehole (Lerouge et al., 2018) seem to support evaporation processes.

Since surface erosion rates are low in the Paris Basin (Prijac et al., 2000), we neglect erosion processes and focus on chemical weathering. We now propose in a first approach to simulate chemically in one dimension the DIC concentrations through the weathering profile developed on Tégulines Clay, using the reactive transport code Phreeqc v3.1.2 (Parkhurst and Appelo, 2013) with the ThermoChimie thermodynamic database (Giffaut et al., 2014).

The initial 1D-model setup considers a 32 m high column (with 1 m meshes) formed of uniformly distributed reduced clay. The column height is approximately the thickness of the clay in the AUB1010 borehole. Initial porosity was 0.25 (Lerouge et al., 2018). Clay pore waters chosen for the model were arbitrarily those of the AUB1010-23 m sample. Indeed, Tégulines Clay is a marine formation, and consequently early pore waters had composition close to seawater. However, the formation has been outcropped since ~23 Ma ago, and meteoric waters have diffused through it since, and diluted the pore waters. The lack of knowledge of the paleogeography and paleoclimate of the area do not allow a running simulation over 23 Ma. In this study, we chose to model scenarios over a period of 10 kyrs, which corresponds to the last ice age, even though the present-day pore-water chemistry is not the same as 10 kyrs ago. Therefore, we assessed the pore waters by equilibration with the calcite-pyrite-goethite- P_{CO_2} assemblage and the clay exchanger, according to the THERMOAR model developed by (Gaucher et al., 2006, 2009). Since the kinetic dissolution of silicate minerals such as quartz and feldspars is much longer than 10 kyrs (Appelo and Postma, 2005; Lasaga, 1984), we simplified the geochemical model focusing on water-rock interactions of calcite and pyrite, and cation exchanges identified in the weathered clay, and assumed silicate minerals to be stable. The surficial waters diffusing through the vertical column considered in the model were natural pore waters in soil (TPH1-1 0–30 cm waters), equilibrated with the atmospheric pressure of oxygen, and taking into account the kinetic reaction of organic matter degradation in soil (Marty et al., 2015, 2018).

The diffusion coefficient was set to $5.10^{-11} \text{ m}^2/\text{s}$ for each ion based on HTO experiments (ANDRA, 2015). There was no consideration of

multi-component diffusion (each ion with its own diffusion coefficient; Hasenmueller et al., 2017).

In a first model, we considered the reactivity in soil and in the clay without evaporation. In that case, the model did not reproduce the DIC curvilinear profile, with high DIC values in the first meters, and ion curvilinear profiles (Fig. 10). Different kinetics values for pyrite oxidation and organic matter degradation did not significantly change the results.

In the second model, we introduced evaporation processes through concentrating surficial waters by approximately six-fold, and adjusted it to DIC measurements. In that way we simulated evaporation processes in the first meter of the clay column (i.e. first cell of the model). This second model reproduced the DIC curvilinear profile defined by core sample degassing quite well and also alkalinities measured on pore waters extracted by squeezing (Fig. 10). This suggests that organic matter degradation in soil and evaporation processes were the major reactions needed to explain the CO_2 anomaly in the 0–10 m zone of the AUB1010 borehole, which is consistent with the CO_2 carbon isotope data, which also show the major contribution of CO_2 derived from organic-matter degradation in soil into this zone. Our model differs on this point from the Opalinus Clay chemical weathering model, where kerogen in the clay formation is considered as the major source of degraded organic matter (Hasenmueller et al., 2017).

Even though the Phreeqc reactive transport modeling at ~10 kyrs reproduced the DIC profile well, the profiles of major ions did not fit so well. Especially chloride concentration was not high enough. Further investigations need to be made in terms of knowledge of paleogeography, hydrology of the system and timing of the processes to explain the discrepancies between the reactive transport model and the data. For chloride and sulfate, discrepancies might be due to some anionic exclusion considered as negligible in Tégulines Clay (Lerouge et al., 2018) and/or to diffusion coefficients different for each ion, as has been demonstrated for Opalinus Clay (Van Loon et al., 2018). In addition, the model does not include how porosity changes with time or the complex water/gas behavior in the unsaturated/saturated zone. Taking into account these parameters might partially solve discrepancies between the model and the data. However, this is beyond the scope of this study; other reactive transport codes (CrunchFlow, TOUGHREACT, MIN3P (Bao et al., 2017; Mayer et al., 2002), or HP1 (Jacques et al., 2008; Šimůnek et al., 2005; Šimůnek et al., 2006) that have been developed to model such hydrogeochemical processes (Li et al., 2017; Steefel et al., 2015) are more suitable for watershed scale modeling.

6. Conclusion

In degassing claystone, monitoring CO_2 , O_2 , N_2 and alkane gas and carbon isotopes on CO_2 we have powerful techniques for defining the depth of the weathering profile in a reduced-marine clay formation. These contribute to a better understanding of weathering processes. In our case study of Tégulines Clay from the eastern part of the Paris Basin, degassed CO_2 significantly increased between 4 and 11 m in the highly reactive transition zone of the weathering profile. The $\delta^{13}C$ of degassed CO_2 provided evidence of the two major CO_2 sources: organic matter degradation and the calcite equilibrium. The increase of degassed CO_2 corresponds both to the degradation of plant roots observed in borehole down to 11 m and to calcite dissolution due to acidic pH (pyrite oxidation, organic matter degradation), due to interactions with oxygen diffusing from atmosphere through the clay. The measurements of CO_2 concentration in the gas phase relative to a volume of degassed clayrock allowed us to estimate the equivalent concentrations of total CO_2 dissolved in clay pore waters that are consistent with total dissolved-carbonate concentration and alkalinity values in clay pore waters extracted by squeezing. Measurements of CO_2 and O_2 partial pressures of constitute key parameters for accurately describing and understanding processes affecting pore water chemistry in the highly reactive transition zone of the weathering profile. Coupled with DIC modeling, those data

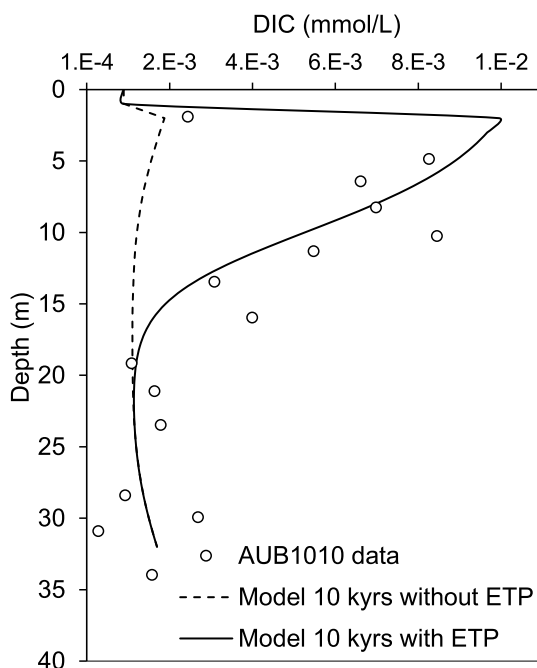


Fig. 10. DIC profile of the AUB1010 borehole compared with reactive transport model of DIC using Phreeqc. ETP: Evapotranspiration.

revealed that evaporation is an additional key parameter to consider in understanding the critical zone and the processes occurring at the redox front. Overall, our results suggest that dissolved gases and their isotopic signatures are good markers of weathering processes in the critical zone.

Declaration of competing interest

The authors declare that they have no known competing financial interests or personal relationships that could have appeared to influence the work reported in this paper.

Acknowledgments

The French National Radioactive Waste Management Agency (ANDRA) and the French Geological Survey (BRGM) supported this study through the GAULT_ZC project. We thank the Associate Editor, Dr Thomas Gimmi, and two anonymous referees for their constructive comments and significant improvements to the manuscript. We are grateful to Dr Karen M. Tkaczyk (McMillan translation) for proofreading and editing the English text.

Appendix A. Supplementary data

Supplementary data to this article can be found online at <https://doi.org/10.1016/j.apgeochem.2020.104573>.

X_i is the concentration (given in volume %) of the i species in the gas phase, P_{total} is the total gas pressure, and V_G is the volume of gas in the glass jar. M and V_R are the mass (in g) and the volume (in L) of rock in the glass jar. W is the water content of the rock (in weight %). $[i]_{(0)}$ and $[i]_{(t)}$ are the initial and final concentrations of the species dissolved in pore waters (given in mmol/L), respectively. In grey, the data that we measure and in red, the data we want to calculate.

References

- Aarão Reis, F.D.A., Brantley, S.L., 2019. The impact of depth-dependent water content on steady state weathering and eroding systems. *Geochem. Cosmochim. Acta* 244, 40–55.
- Amédéo, F., Matrimon, B., Magniez-Jannin, F., Touch, R., 2014. La limite Albien inférieur-Albien moyen dans l'Albien type de l'Aube (France): ammonites, foraminifères, séquences. *Rev. Paléobiol.* 33, 159–279.
- ANDRA, 2015. PNGMDR 2013-2015 Projet de stockage de déchets radioactifs de faible activité massique à vie longue (FA-VL) Rapport d'étape 2015. <https://www.andra.fr/sites/default/files/2018-01/rapport-etape-fav1.pdf>.
- Appelo, C., Postma, D., 2005. *Geochemistry, Groundwater and Pollution*. CRC, Balkema, Rotterdam.
- Bao, Z., Haberger, C.M., Maier, U., Amos, R.T., Blowes, D.W., Gratwohl, P., 2017. Modeling controls on the chemical weathering of marine mudrocks from the Middle Jurassic in Southern Germany. *Chemical Geology* 459, 1–12.
- Bolton, E.W., Berner, R.A., Petsch, S.T., 2006. The weathering of sedimentary organic matter as a control on atmospheric O₂: II. Theoretical modeling. *Am. J. Sci.* 306, 575–615.
- Brantley, S.L., Goldhaber, M.B., Ragnarsdóttir, K.V., 2007. Crossing disciplines and scales to understand the critical zone. *Elements* 3, 307–314.
- Brantley, S.L., Holleran, M.E., Jin, L., Bazilevskaya, E., 2013. Probing deep weathering in the Shale Hills Critical Zone Observatory, Pennsylvania (USA): the hypothesis of nested chemical reaction fronts in the subsurface. *Earth Surf. Process. Landforms* 38, 1280–1298.
- Debure, Mathieu, Grangeon, Sylvain, Robinet, Jean-Charles, Madé, Benoît, Fernández, Ana-Maria, Lerouge, Catherine, 2020. Influence of soil redox state on mercury sorption and reduction capacity. *Science of The Total Environment* 707 (10), 1–9, 136069. <https://doi.org/10.1016/j.scitotenv.2019.136069>.
- Debure, M., Tournassat, C., Lerouge, C., Madé, B., Robinet, J.-C., Fernández, A.M., Grangeon, S., 2018. Retention of arsenic, chromium and boron on an outcropping clay-rich rock formation (the Tégulines Clay, eastern France). *Sci. Total Environ.* 642, 216–229.
- Deines, P., Langmuir, D., Harmon, R.S., 1974. Stable carbon isotope ratios and the existence of a gas phase in the evolution of carbonate ground waters. *Geochem. Cosmochim. Acta* 38, 1147–1164.
- Dideriksen, K., Christiansen, B.C., Baker, J.A., Frandsen, C., Balic-Zunic, T., Tullborg, E., Mørup, S., Stipp, S.L.S., 2007. Fe-oxide fracture fillings as a palaeo-redox indicator: structure, crystal form and Fe isotope composition. *Chem. Geol.* 244, 330–343.
- Drake, H., Tullborg, E.-L., MacKenzie, A.B., 2009. Detecting the near-surface redox front in crystalline bedrock using fracture mineral distribution, geochemistry and U-series disequilibrium. *Appl. Geochem.* 24, 1023–1039.
- Duffy, C., Shi, Y., Davis, K., Slingerland, R., Li, L., Sullivan, P.L., Goddérís, Y., Brantley, S. L., 2014. Designing a suite of models to explore critical zone function. *Procedia Earth Planet. Sci.* 10, 7–15.
- Fernández, A.M., Sánchez-Ledesma, D.M., Tournassat, C., Melón, A., Gaucher, E.C., Astudillo, J., Vinsot, A., 2014. Applying the squeezing technique to highly consolidated clayrocks for pore water characterisation: lessons learned from experiments at the Mont Terri Rock Laboratory. *Appl. Geochem.* 49, 2–21.
- Gaucher, É.C., Blanc, P., Bardot, F., Braibant, G., Buschaert, S., Crouzet, C., Gautier, A., Girard, J.-P., Jacquot, E., Lassin, A., Negrel, G., Tournassat, C., Vinsot, A., Altmann, S., 2006. Modelling the porewater chemistry of the Callovian–Oxfordian formation at a regional scale. *Compt. Rendus Geosci.* 338, 917–930.
- Gaucher, E.C., Lassin, A., Lerouge, C., Fléhoc, C., Marty, N.C.M., Henry, B., Tournassat, C., Altmann, S., Vinsot, A., Buschaert, S., Matray, J.M., Leupin, O.X., De Craen, M., 2010. CO₂ Partial Pressure in Clayrocks: a General Model, Water-Rock Interaction WRI-13. Taylor & Francis Group (CRC Press), Guanajuato, Mexico, pp. 855–858.
- Gaucher, E.C., Tournassat, C., Pearson, F.J., Blanc, P., Crouzet, C., Lerouge, C., Altmann, S., 2009. A robust model for pore-water chemistry of clayrock. *Geochem. Cosmochim. Acta* 73, 6470–6487.
- Giffaut, E., Grivé, M., Blanc, P., Vieillard, P., Colàs, E., Gailhanou, H., Gaboreau, S., Marty, N., Made, B., Duro, L., 2014. Andra thermodynamic database for performance assessment: ThermoChimie. *Appl. Geochem.* 49, 225–236.
- Girard, J.-P., Fléhoc, C., Gaucher, E., 2005. Stable isotope composition of CO₂ outgassed from cores of argillites: a simple method to constrain $\delta^{18}\text{O}$ of porewater and $\delta^{13}\text{C}$ of dissolved carbon in mudrocks. *Appl. Geochem.* 20, 713–725.
- Hasenmueller, E.A., Gu, X., Weitzman, J.N., Adams, T.S., Stinchcomb, G.E., Eissenstat, D. M., Drohan, P.J., Brantley, S.L., Kaye, J.P., 2017. Weathering of rock to regolith: the activity of deep roots in bedrock fractures. *Geoderma* 300, 11–31.
- Heidari, P., Li, L., Jin, L., Williams, J.Z., Brantley, S.L., 2017. A reactive transport model for Marcellus shale weathering. *Geochem. Cosmochim. Acta* 217, 421–440.
- Hendry, M.J., Wassenaar, L.L., 2000. Controls on the distribution of major ions in pore waters of a thick surficial aquitard. *Water Resour. Res.* 36, 503–513.
- Jacques, D., Simunek, J., Mallants, D., Van Genuchten, M.T., 2008. Modeling coupled hydrologic and chemical processes: Long-term uranium transport following phosphorus fertilization. *Vadose Zone Journal* 7, 698–711.
- Jin, L., Brantley, S.L., 2011. Soil chemistry and shale weathering on a hillslope influenced by convergent hydrologic flow regime at the Susquehanna/Shale Hills Critical Zone Observatory. *Appl. Geochem.* 26, S51–S56.
- Jin, L., Ravella, R., Ketchum, B., Bierman, P.R., Heaney, P., White, T., Brantley, S.L., 2010. Mineral weathering and elemental transport during hillslope evolution at the susquehanna/shale hills critical zone observatory. *Geochem. Cosmochim. Acta* 74, 3669–3691.
- Kim, H.-C., Lee, K., 2009. Significant Contribution of Dissolved Organic Matter to Seawater Alkalinity.
- Lasaga, A.C., 1984. Chemical kinetics of water-rock interactions. *J. Geophys. Res.: Solid Earth* 89, 4009–4025.
- Lebedeva, M.I., Fletcher, R.C., Balashov, V.N., Brantley, S.L., 2007. A reactive diffusion model describing transformation of bedrock to saprolite. *Chem. Geol.* 244, 624–645.
- Lerouge, C., Blessing, M., Fléhoc, C., Gaucher, E.C., Henry, B., Lassin, A., Marty, N., Matray, J.M., Proust, E., Rufer, D., Tremosa, J., Vinsot, A., 2015. Dissolved CO₂ and alkane gas in clay formations. *Procedia Earth Planet. Sci.* 13, 88–91.
- Lerouge, C., Claret, F., Tournassat, C., Grangeon, S., Gaboreau, S., Boyer, B., Borschnek, D., Linard, Y., 2014. Constraints from sulfur isotopes on the origin of gypsum at concrete/claystone interfaces. *Phys. Chem. Earth, Parts A/B/C* 70–71, 84–95.
- Lerouge, C., Grangeon, S., Gaucher, E.C., Tournassat, C., Agrinier, P., Guerrot, C., Widory, D., Fléhoc, C., Wille, G., Ramboz, C., Vinsot, A., Buschaert, S., 2011. Mineralogical and isotopic record of biotic and abiotic diagenesis of the Callovian–Oxfordian clayey formation of Bure (France). *Geochem. Cosmochim. Acta* 75, 2633–2663.
- Lerouge, C., Robinet, J.-C., Debure, M., Tournassat, C., Bouchet, A., Fernandez, A.M., Fléhoc, C., Guerrot, C., Kars, M., Lagroix, F., Landrein, P., Madé, B., Negrel, P., Wille, G., Claret, F., 2018. A deep alteration and oxidation profile in a shallow clay aquitard: example of the tégulines clay, east Paris basin, France. *Geofluids* 2018, 20.
- Li, L., Maher, K., Navarre-Sitchler, A., Druhan, J., Meile, C., Lawrence, C., Moore, J., Perdrial, J., Sullivan, P., Thompson, A., Jin, L., Bolton, E.W., Brantley, S.L., Dietrich, W.E., Mayer, K.U., Steefel, C.I., Valocchi, A., Zachara, J., Kocar, B., McIntosh, J., Tutolo, B.M., Kumar, M., Sonnenthal, E., Bao, C., Beisman, J., 2017. Expanding the role of reactive transport models in critical zone processes. *Earth Sci. Rev.* 165, 280–301.
- Marty, N.C., Claret, F., Lassin, A., Tremosa, J., Blanc, P., Madé, B., Giffaut, E., Cochebin, B., Tournassat, C., 2015. A database of dissolution and precipitation rates for clay-rocks minerals. *Appl. Geochem.* 55, 108–118.
- Marty, N.C., Lach, A., Lerouge, C., Grangeon, S., Claret, F., Fauchet, C., Madé, B., Lundy, M., Lagroix, F., Tournassat, C., 2018. Weathering of an argillaceous rock in the presence of atmospheric conditions: a flow-through experiment and modelling study. *Appl. Geochem.* 96, 252–263.
- Mayer, K.U., Frind, E.O., Blowes, D.W., 2002. Multicomponent reactive transport modeling in variably saturated porous media using a generalized formulation for kinetically controlled reactions. *Water Resources Research* 38, 1311–1321.
- Mazurek, M., Alexander, W.R., MacKenzie, A.B., 1996. Contaminant retardation in fractured shales: matrix diffusion and redox front entrapment. *J. Contam. Hydrol.* 21, 71–84.
- Mook, W.G., Bommerson, J.C., Staverman, W.H., 1974. Carbon isotope fractionation between dissolved bicarbonate and gaseous carbon dioxide. *Earth Planet Sci. Lett.* 22, 169–176.

- Parkhurst, D.L., Appelo, C.A.J., 2013. Description of Input and Examples for PHREEQC Version 3—a Computer Program for Speciation, Batch-Reaction, One-Dimensional Transport, and Inverse Geochemical Calculations.
- Prijac, C., Doin, M.P., Gaulier, J.M., Guillocheau, F., 2000. Subsidence of the Paris Basin and its bearing on the late Variscan lithosphere evolution: a comparison between Plate and Chablis models. *Tectonophysics* 323, 1–38.
- Schaap, M.G., Leij, F.J., Van Genuchten, M.T., 2001. Rosetta: a computer program for estimating soil hydraulic parameters with hierarchical pedotransfer functions. *J. Hydrol.* 251, 163–176.
- Šimůnek, J., Jacques, D., Van Genuchten, M.T., Mallants, D., 2006. Multicomponent geochemical transport modeling using HYDRUS-1D and HP1. *Am. Water Resour. Assoc.* 42, 1537–1547.
- Šimůnek, J., Van Genuchten, M.T., Sejna, M., 2005. The HYDRUS-1D software package for simulating the one-dimensional movement of water, heat, and multiple solutes in variably-saturated media. University of California-Riverside Research Reports 3, 1–240.
- Soulet, G., Hilton, R.G., Garnett, M.H., Dellinger, M., Croissant, T., Ogrič, M., Klotz, S., 2018a. In situ measurement of flux and isotopic composition of CO₂ released during oxidative weathering of sedimentary rocks. *Biogeosciences* 15, 4087–4102.
- Steeffel, C.I., Appelo, C.A.J., Arora, B., Jacques, D., Kalbacher, T., Kolditz, O., Lagneau, V., Lichtner, P.C., Mayer, K.U., Meeussen, J.C.L., Molins, S., Moulton, D., Shao, H., Šimůnek, J., Spycher, N., Yabusaki, S.B., Yeh, G.T., 2015. Reactive transport codes for subsurface environmental simulation. *Comput. Geosci.* 19, 445–478.
- Sullivan, P.L., Ma, L., West, N., Jin, L., Karwan, D.L., Noireaux, J., Steinhoefel, G., Gaines, K.P., Eissenstat, D.M., Gaillardet, J., Derry, L.A., Meek, K., Hynek, S., Brantley, S.L., 2016. CZ-tope at Susquehanna Shale Hills CZO: synthesizing multiple isotope proxies to elucidate Critical Zone processes across timescales in a temperate forested landscape. *Chem. Geol.* 445, 103–119.
- Torres, M.A., West, A.J., Li, G., 2014. Sulphide oxidation and carbonate dissolution as a source of CO₂ over geological timescales. *Nature* 507, 346–349.
- Tostevin, R., Shields, G.A., Tarbuck, G.M., He, T., Clarkson, M.O., Wood, R.A., 2016. Effective use of cerium anomalies as a redox proxy in carbonate-dominated marine settings. *Chem. Geol.* 438, 146–162.
- Tremosa, J., Arcos, D., Matray, J.M., Bensenouci, F., Gaucher, E.C., Tournassat, C., Hadi, J., 2012. Geochemical characterization and modelling of the Toarcian/Domerian porewater at the Tournemire underground research laboratory. *Appl. Geochem.* 27, 1417–1431.
- Tuttle, M.L.W., Breit, G.N., 2009. Weathering of the New Albany Shale, Kentucky, USA: I. Weathering zones defined by mineralogy and major-element composition. *Appl. Geochem.* 24, 1549–1564.
- Tuttle, M.L.W., Breit, G.N., Goldhaber, M.B., 2009. Weathering of the new albania shale, Kentucky: II. Redistribution of minor and trace elements. *Appl. Geochem.* 24, 1565–1578.
- Van Loon, L.R., Leupin, O.X., Cloet, V., 2018. The diffusion of SO₄²⁻ in Opalinus Clay: measurements of effective diffusion coefficients and evaluation of their importance in view of microbial mediated reactions in the near field of radioactive waste repositories. *Appl. Geochem.* 95, 19–24.
- Wersin, P., Mazurek, M., Mäder, U.K., Gimmi, T., Rufer, D., Lerouge, C., Traber, D., 2016. Constraining porewater chemistry in a 250 m thick argillaceous rock sequence. *Chem. Geol.* 434, 43–61.
- White, T., Brantley, S., Banwart, S., Chorover, J., Dietrich, W., Derry, L., Lohse, K., Anderson, S., Aufdenkampe, A., Bales, R., Kumar, P., Richter, D., McDowell, B., 2015. Chapter 2 - the role of critical zone observatories in critical zone science. In: Giardino, J.R., Houser, C. (Eds.), *Developments in Earth Surface Processes*. Elsevier, pp. 15–78.
- Yesavage, T., Fantle, M.S., Vervoort, J., Mathur, R., Jin, L., Liermann, L.J., Brantley, S.L., 2012. Fe cycling in the Shale Hills Critical Zone Observatory, Pennsylvania: an analysis of biogeochemical weathering and Fe isotope fractionation. *Geochem. Cosmochim. Acta* 99, 18–38.
- Yu, C., Drake, H., Mathurin, F.A., Åström, M.E., 2017. Cerium sequestration and accumulation in fractured crystalline bedrock: the role of Mn-Fe (hydr)-oxides and clay minerals. *Geochem. Cosmochim. Acta* 199, 370–389.